Geo-Mar Lett (2016) 36:51–66
DOI 10.1007/s00367-015-0426-2

ORIGINAL

# Holocene Climatic Optimum centennial-scale paleoceanography in the NE Aegean (Mediterranean Sea)

**Maria V. Triantaphyllou**[1] **· Alexandra Gogou**[2] **· Margarita D. Dimiza**[1] **· Sofia Kostopoulou**[1] **· Constantine Parinos**[2] **· Grigoris Roussakis**[2] **· Maria Geraga**[3] **· Ioanna Bouloubassi**[4] **· Dominik Fleitmann**[5] **· Vassilis Zervakis**[6] **· Dimitris Velaoras**[2] **· Antonia Diamantopoulou**[3] **· Angeliki Sampatakaki**[2] **· Vassilis Lykousis**[2]

Received: 3 June 2015 / Accepted: 30 September 2015 / Published online: 9 October 2015


**Abstract** Combined micropaleontological and geochemical analyses of the high-sedimentation gravity core M-4G provided new centennial-scale paleoceanographic data for sapropel S1 deposition in the NE Aegean Sea during the Holocene Climatic Optimum. Sapropel layer S1a (10.2–8.0 ka) was deposited in dysoxic to oxic bottom waters characterized by a high abundance of benthic foraminiferal species tolerating surface sediment and/or pore water oxygen depletion (e.g., *Chilostomella mediterranensis*, *Globobulimina affinis*), and the presence of *Uvigerina mediterranea*, which thrives in oxic mesotrophic-eutrophic environments. Preservation of organic matter (OM) is inferred based on high organic carbon as well as loliolide and isololiolide contents, while the biomarker record and the abundances of eutrophic planktonic foraminifera document enhanced productivity. High inputs of terrigenous OM are attributed to north Aegean borderland riverine inputs. Both alkenone-based sea surface temperatures (SSTs) and $\delta O^{18}{}_{G.\ bulloides}$ records indicate cooling at 8.2 ka (S1a) and ~7.8 ka (S1 interruption). Sapropelic layer S1b (7.7–6.4 ka) is characterized by rather oxic conditions; abundances of foraminiferal species tolerant to oxygen depletion are very low compared with the *U. mediterranea* rise. Strongly fluctuating SSTs demonstrate repeated cooling and associated dense water formation, with a major event at 7.4 ka followed by cold spells at 7.0, 6.8, and 6.5 ka. The prominent rise of the carbon preference index within the S1b layer indicates the delivery of less degraded terrestrial OM. The increase of algal biomarkers, labile OM-feeding foraminifera and eutrophic planktonic species pinpoints an enhanced in situ marine productivity, promoted by more efficient vertical convection due to repeated cold events. The associated contributions of labile marine OM along with fresher terrestrial OM inputs after ~7.7 ka imply sources alternative/additional to the north Aegean riverine borderland sources for the influx of organic matter in the south Limnos Basin, plausibly related to the inflow of highly productive Marmara/Black Sea waters.

**Electronic supplementary material** The online version of this article (doi:10.1007/s00367-015-0426-2) contains supplementary material, which is available to authorized users.

✉ Maria V. Triantaphyllou
mtriant@geol.uoa.gr

1 Faculty of Geology and Geoenvironment, National and Kapodistrian University of Athens, 15784Panepistimioupolis, Athens, Greece

2 Hellenic Centre for Marine Research, Institute of Oceanography, 19013 Anavyssos, Attiki, Greece

3 Laboratory of Marine Geology and Physical Oceanography, Department of Geology, University of Patras, 26100, Rion-Patra, Greece

4 Laboratoire d'Océanographie et du Climat, Expérimentation et Approche Numérique, Université Pierre et Marie Curie, Paris Cedex 05, France

5 Centre for Past Climate Change, Department of Archaeology, University of Reading, Reading RG6 6AB, UK

6 Department of Marine Sciences, University of the Aegean, 81100 Mytilene-Lesvos, Greece

## Introduction

The Aegean Sea (NE Mediterranean) is located in a transition zone between temperate and semiarid climate conditions and is characterized by its small size but complex bathymetry. Fluvial freshwater inputs are more intense in the north due to numerous large rivers draining from the Balkans and Turkey, which provide 75% of sediment influx into the north Aegean (e.g., Lykousis et al. 2002; Roussakis et al. 2004). River runoff collectively constitutes an important source of land-derived organic matter (OM) to the study area (e.g., Gogou et al. 2007).

In general, sapropels have developed in concert with distinct minima in the orbital precession (e.g., Rossignol-Strick et al. 1982) when intensification of the western African monsoon caused an increased freshwater discharge of north African rivers into the eastern Mediterranean (e.g., Rohling et al. 2002a, 2015). Sapropel S1 was deposited in the period 10.8–6.1 ka (De Lange et al. 2008) and was terminated with earlier ventilation at water depths shallower than 1,800 m (Tachikawa et al. 2015); deep-water anoxia required a long prelude of deep-water stagnation, with no particularly strong eutrophication (Grimm et al. 2015).

During the so-called Holocene Climatic Optimum (HCO; approx. 10.0–6.0 ka), a distinct positive shift in the Aegean Sea's freshwater budget—possibly supplemented by precipitation and riverine contribution from the Aegean borderland and also inflow of Black Sea Water (BSW)—weakened the basin's deepwater circulation, resulting in oxygen-starved conditions at the seafloor and deposition of sapropel layer S1 (e.g., Aksu et al. 1995, 2002; Gogou et al. 2007; Kuhnt et al. 2007; Abu-Zied et al. 2008; Kotthoff et al. 2008; Geraga et al. 2010; Katsouras et al. 2010; Schmiedl et al. 2010; Kouli et al. 2012; Triantaphyllou 2014; Triantaphyllou et al. 2014). Aegean Sea sites of high sedimentation rates are associated with S1 sapropelic layers characterized by low organic carbon (OC) contents of <2% (e.g., Roussakis et al. 2004; Triantaphyllou et al. 2009a), reflecting strong dilution by lithogenic input (e.g., Mercone et al. 2000). A multi-centennial climate deterioration (Rohling et al. 2002b; Rohling and Pälike 2005; Marino et al. 2009) with a superimposed abrupt "8.2 ka" event (Alley et al. 1997) is associated with the S1 interruption, and has been ascribed to an overturning reinforcement and reventilation of deep waters (e.g., Myers and Rohling 2000; Casford et al. 2003).

Concerning the age of the last reconnection of the Black Sea with waters of Mediterranean origin, several datings have been proposed. Ryan et al. (2003) and Major et al. (2006) provided an age of 8.4 thousand years BP (~9.0 ka; Soulet et al. 2011; Mertens et al. 2012). Hiscott et al. (2007) dated the initial marine inflow at 11,340±80 years BP (~12.8 ka). A late connection has been suggested to have occurred between 9.0 and 8.0 ka (Sperling et al. 2003; Bahr et al. 2006; Major et al. 2006; Vidal et al. 2010). Adding to this, data provided by the Holocene section of the Sofular Cave speleothem record from the southern Black Sea coast indicate a remarkable increase in rainfall between ~9.6 and 5.4 ka (Göktürk et al. 2011).

Despite the fact that significant work has been done on the paleoceanography of the north Aegean (for references, see above), there is still a lack of detailed information based on a north Aegean sediment record reconstructing a possible Marmara/BSW influence in the Aegean Sea/NE Mediterranean during the early and middle Holocene. Previous studies (e.g., Schmiedl et al. 2010; Triantaphyllou 2014) have considered this issue; however, they did not examine records in the direct vicinity of BSW pathways. To address this aspect, the present work investigated high-resolution micropaleontological (benthic and planktonic foraminifera) and geochemical signatures (OC, stable isotopes, selected lipid biomarkers and their diagnostic ratios, and the alkenone unsaturation index $U^{K'}_{37}$ as proxy of sea surface temperature) in the excellently preserved S1 sapropelic layers of gravity core M-4G from the south Limnos Basin (Fig. 1a, b).

Benthic foraminifera are commonly used as proxies of the trophic level at the sediment–water interface and oxygen concentration of deep waters (e.g., Jorissen et al. 1992). *Chilostomella mediterranensis*, *Globobulimina affinis* and *Cassidulinoides bradyi* represent benthic foraminiferal species able to tolerate oxygen depletion (e.g., Bernard and Sen Gupta 1999; Fontanier et al. 2002; Kuhnt et al. 2007; Abu-Zied et al. 2008). However, *G. affinis*, *C. mediterranensis*, *Bulimina* spp. and *Bolivina spathulata* also thrive in OM-enriched but well-oxygenated ecosystems, indicating low-oxygen conditions prevailing in pore water (Duchemin et al. 2007; Fontanier et al. 2008a, 2008b, 2014). Likewise, planktonic foraminifera have long proven useful in the reconstruction of paleoceanographic and paleoclimatic conditions worldwide (e.g., Pujol and Vergnaud Grazzini 1995; Schiebel et al. 2001; Mojtahid et al. 2013), and several studies are available from the Aegean Sea (e.g., Geraga et al. 2000, 2005, 2010; Casford et al. 2007; Triantaphyllou et al. 2009b).

Moreover, lipid biomarkers such as long-chain alkenones and dinosterol biosynthesized by the prymnesiophytes *Emiliania huxleyi* and *Gephyrocapsa* spp. and dinoflagellates, respectively (Marlowe et al. 1984; Volkman 1986) can serve as indicators of marine productivity (e.g., Gogou et al. 2007). Loliolide and isololiolide are known to be produced after degradation of the pigment fucoxanthin present in diatoms and haptophytes (Repeta 1989) under dysoxic/anoxic bottom water conditions (e.g., formation of Mediterranean sapropels; Menzel et al. 2003; Triantaphyllou et al. 2009a). Elevated levels of Ter-alkanols, and concomitant increase in their carbon preference index (CPI) values, are well known in Mediterranean sapropels, and have been ascribed a terrestrial origin from leaf waxes of higher plants during increased land runoff (e.g., Gogou et al. 2007 and references therein).

Within this context, the present study aims to (1) construct a high-resolution paleoceanographic record for the NE Aegean Sea during the HCO, and (2) investigate the influence of paleoclimatic forcings and BSW influx on the NE Aegean paleoceanography. It was expected that the shallow water depth (216 m) of the study site would facilitate the reconstruction of rapid water-column processes affecting the physical and biogeochemical regimes of the north Aegean Sea.

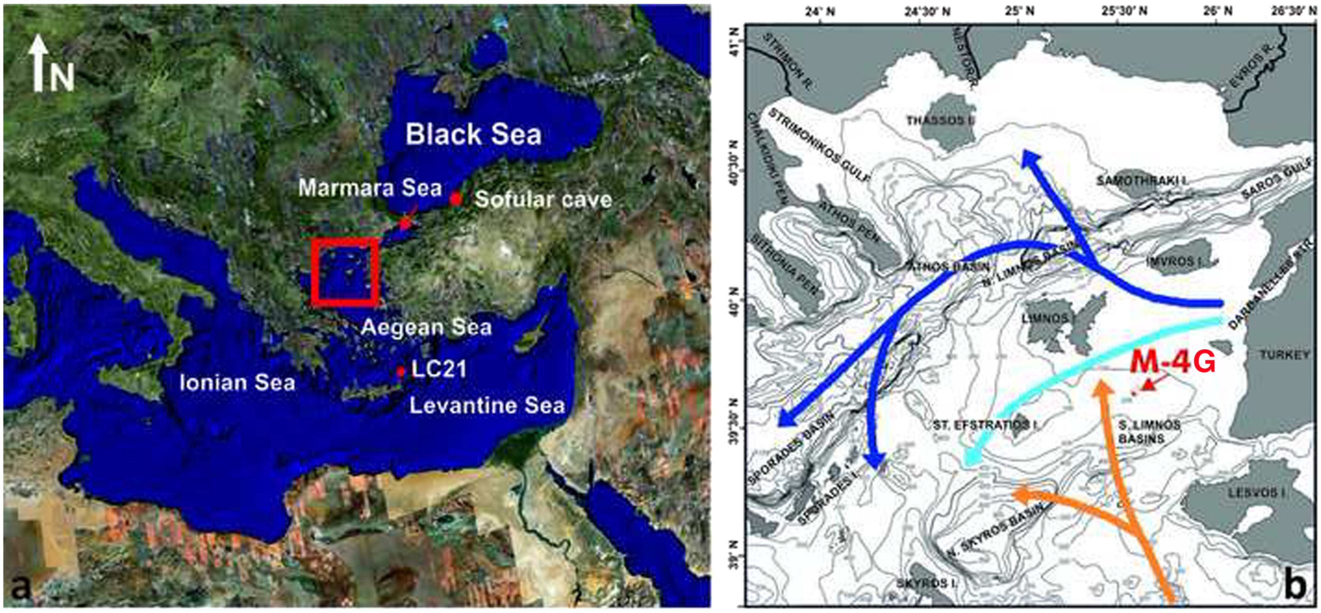


**Fig. 1** **a** Location map of the study area and the sites discussed in the text (source: Google Earth, 2015, www.google.com/maps/). **b** Geographical location of the studied core M-4G in the NE Aegean Sea, and the main patterns of seawater surface circulation: BSW main pathways during winter (*dark blue*) and additional pathway during summer (*light blue*). *Yellow arrows* Routes of high-salinity water masses of Levantine origin toward the north Aegean

## Oceanographic setting

The north Aegean basin presents a continental margin ecosystem with a generally cyclonic circulation and dual flow between the NE Mediterranean and Black seas through the Dardanelles and Bosphorus straits (Fig. 1a). The north Aegean Sea is considered as one of the most important areas for dense water formation in the eastern Mediterranean region (e.g., Theocharis and Georgopoulos 1993; Zervakis et al. 2000; Velaoras and Lascaratos 2005; Theocharis et al. 2014; Velaoras et al. 2014).

Low-salinity (24–28‰ at the strait mouth, <70 m depth) surface BSW flows along the eastern coast of Greece until it reaches the southwestern Aegean, and enhances productivity in the northern Aegean Sea (Lykousis et al. 2002). During winter (Figs. 1b, 2a), BSW tends to flow northwest of Limnos filling the northernmost part of the Aegean before moving westward (Lascaratos 1992; Zodiatis 1994). The low-density BSW surface layer acts as an insulating lid that impedes air–sea interactions, resulting in the stratification of the water column and hindering dense water formation over the area it covers (Zervakis et al. 2000; Velaoras et al. 2013). During summer, the strong northerly winds (Etesians) blowing over the Aegean Sea deflect the BSW to some extent south of Limnos (Zodiatis 1994), and cause a thermal front marked by low sea surface temperatures (SSTs; Fig. 2b) due to upwelling of colder, nutrient-rich masses along the eastern Aegean margin (e.g., Lascaratos 1992). BSW inflow rates show strong seasonal and interannual variability, reaching a maximum during mid to late summer and a minimum during winter (Zervakis et al. 2000). Warmer than the surrounding surface masses, saline (>39‰) Levantine Surface Water (LSW) occupies surface layers in the absence of BSW, and Levantine Intermediate Water (LIW; 14–15 °C, 38.8–39.1‰) extends to a depth of up to about 400 m below the BSW/LSW. These Levantine water masses flow northward along the eastern Aegean Sea (e.g., Zervakis et al. 2004).

Among the north Aegean basins, the Limnos Basin, located closest to the Dardanelles exit, is strongly influenced by BSW outflow. The Limnos Plateau, between the islands of Limnos, Imvros and Lesvos (Fig. 1b), is characterized by the formation of dense water during winter, although this can be reduced by BSW. These dense waters ventilate intermediate layers up to a few hundred meters deep, and occasionally even bottom layers in the north Limnos and Skyros basins (e.g., Theocharis and Georgopoulos 1993).

## Materials, methods, age model

### Core location and description

The 2.53-m-long gravity core M-4G (39°38.662′N, 25°35.165′E) was recovered from the south Limnos Basin (Fig. 1b) at a water depth of 216 m within the framework of the MedEcos project (R/V Aegaeo, January 2011), from exactly the same location as that of core M-4 investigated by Roussakis et al. (2004). Notably, the core site represents an isolated depression on the shallower (100 m depth) Limnos Plateau (Fig. 1b, see arrow). In the laboratory, the core was

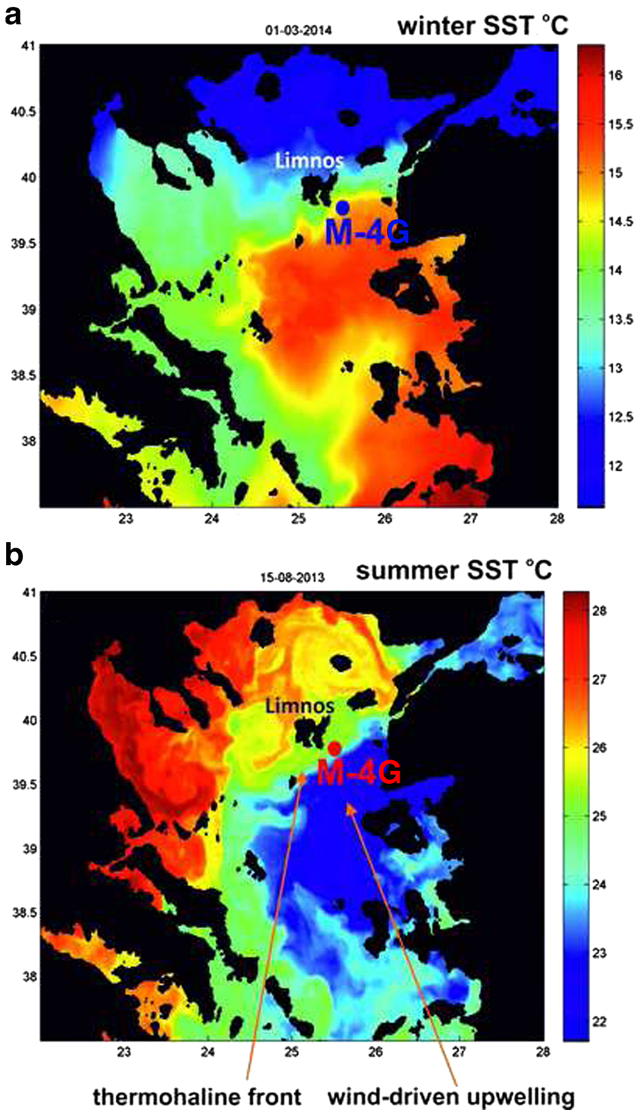


**Fig. 2** **a** 1 March 2014 satellite SST image with a typical winter SST distribution over the north-central Aegean. Cold water masses restricted north of Limnos show BSW expansion in the north Aegean during winter. **b** 15 August 2013 satellite SST image with a typical summer SST distribution. The thermohaline front is located south of Limnos with a southwest orientation. BSW occupies the area north of the front. Colder surface water masses south of the front (eastern part of Aegean basin) are attributed to wind-driven upwelling due to summer Etesian winds (source: MyOcean MED Sea Surface Temperature maps at ultra-high (0.01°) spatial resolution, www.myocean.eu)

split, macroscopically described, and subsampled downcore at 0.5 cm intervals.

Core M-4G is described here following the lithological units of Roussakis et al. (2004). The top 23 cm (Fig. 3a) consists of grayish olive (7.5 Y5/2) mud with shells and shell fragments, followed by a thin layer (23–32 cm depth) of olive gray (2.5 GY5/1) mud strongly bioturbated in its upper part, with numerous *Ostrea* valves. These form unit A (late Holocene mud). The underlying unit (32–128 cm depth) consists of three sublayers forming unit B (sapropel S1 sequence): a homogeneous olive gray (10 Y5/2) sapropelic mud layer (S1a, 32–54 cm depth) with faint laminations, followed by a light-colored interval (S1 interruption S1i, 54–59 cm depth) of olive gray (2.5 GY5/1) mud, and a thick layer (S1b, 59–128 cm depth) of olive gray (10 Y4/2) laminated sapropelic muds that comprise a lighter-colored faintly laminated layer of sapropelic mud (grayish olive, 7.5 GY5/1) at 118–128 cm depth. The whole of unit B does not display any burrows or other signs of bioturbation. The remainder of the core comprises unit C (deglaciation mud and sandy mud). The 128–142 cm depth interval consists of olive gray (2.5 GY5/1) mud, whereas olive gray (2.5 GY6/1) mud with bivalve shells and lenses of silt occurs at 142–162 cm. From 162 to 245 cm depth, the sediments consist of olive gray (2.5 GY5/1, 4/1) stiff mud characterized by organic remains and sand lenses with shell fragments. These turbiditic sand lenses probably originate from slope gravity flows during the last sea-level lowstand. The bottom 15 cm of the core comprises grayish olive (7.5 Y5/2) very stiff muddy sand.

In this study only the interval comprising the S1 sequence is examined. S1 sapropelic layers are very well preserved between 32–128 cm (Fig. 3a), enabling a high-resolution examination.

## Chronology

Four accelerator mass spectrometry (AMS) radiocarbon $^{14}C$ datings (Table 1) were performed on clean, handpicked mixed planktonic foraminiferal surface-water dwellers (*Globigerina bulloides*, *Globigerinoides ruber*) at the laboratories of the oceanographic institute LOCEAN, Université P. & M. Curie, Paris. Conventional $^{14}C$ ages were calibrated by means of the Calib version 7.0.2 software (Stuiver and Reimer 1993) and the MARINE13 dataset with a regional reservoir age correction (ΔR) of 139±40 years for the S1 sapropel interval (Facorellis et al. 1998), and 58±85 years outside this interval (Reimer et al. 2013). Hereafter the M-4G calibrated ages are reported as ka.

The chronology for core M-4G derives from a satisfactory polynomial fit through the four calibrated AMS $^{14}C$ datings mentioned above, with 1σ uncertainty of ±0.044 ka (Fig. 3b). Sapropelic layer S1a is dated 10.2–8.0 ka, whereas S1b spans the interval 7.7–6.4 ka. The temporal resolution is ~30 years for S1a, ~45 years for S1i, and ~50 years for S1b. Comparison with the multi-proxy chronological framework proposed by Casford et al. (2007), i.e., primary events based on changes in planktonic fauna (events 5, 6, 7) in the reference core LC21 (35°40′N, 26°35′E, 1,522 m water depth northeast of Crete; Fig. 1a), revealed an excellent match (Fig. 3b). Core LC21 is the benchmark against which Casford et al. (2007) constructed a robust chronology within the early

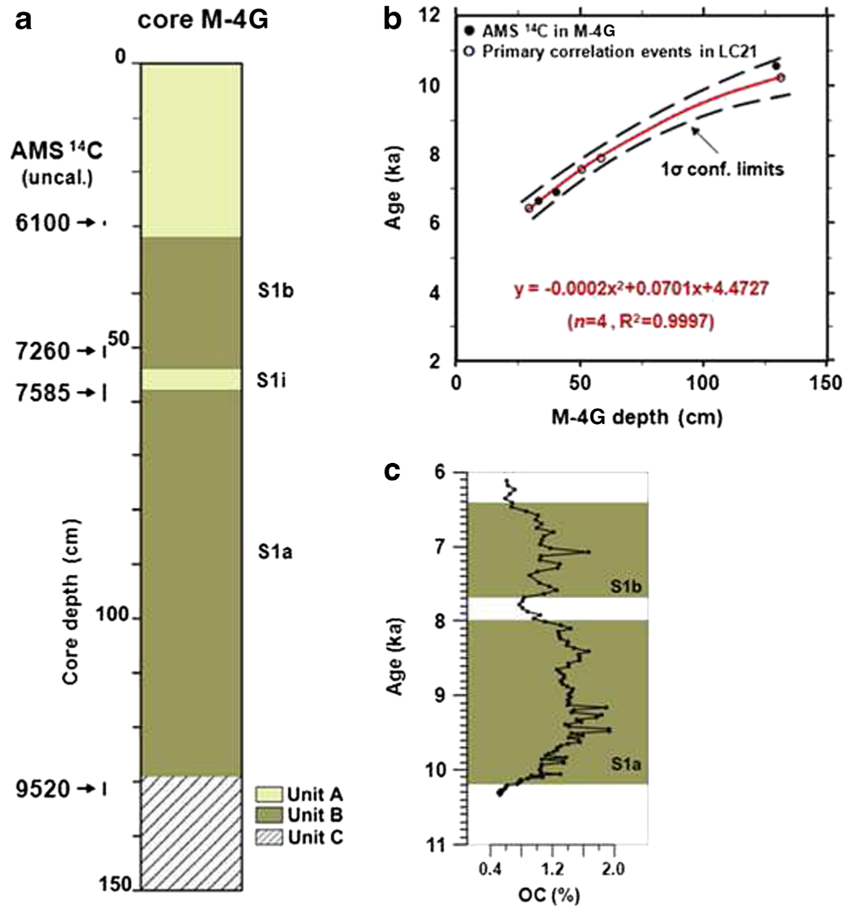


**Fig. 3** **a** Gravity core M-4G stratigraphy (upper 150 cm, lithological description follows Roussakis et al. 2004) and uncalibrated AMS $^{14}$C datings (years BP). **b** Age model for core M-4G, based on a 2nd-order polynomial fit for the four youngest calibrated AMS $^{14}$C datings (red line, open dots). *Solid dots* Ages for the reference core LC21 extracted from Casford et al. (2007). For more information, see main text. **c** OC (%). *Shaded areas* Periods of deposition of S1a and S1b layers

to middle Holocene interval, involving numerous Aegean cores.

## Organic carbon

In all, 230 subsamples were collected at 0.5 cm intervals for OC analyses at the University of California, Davis. Freeze-dried and homogenized aliquots were de-carbonated using repetitive additions of HCl (25%, v/v) combined with 60 °C drying steps. OC was determined by combustion in an oxygen atmosphere, and the produced carbon dioxide was quantitatively measured on a PDZ Europa ANCA-GSL elemental analyzer coupled with a PDZ Europa 20-20 IRMS instrument. The analytical precision was in the order of ±0.02%.

## Benthic and planktonic foraminifera

For benthic foraminiferal analyses (see Appendix A in the electronic supplementary material available online for this article), 71 sediment samples (ca. 2 cm sampling resolution, 2 g dry weight each) were disaggregated using hydrogen peroxide, and then wet sieved through a 125 μm mesh. The dry material was split into aliquots using an Otto microsplitter. In each case, at least 300 specimens were separated under a Leica APO S8 stereoscope.

The taxonomy of benthic foraminifers is based on original descriptions in Ellis and Messina (1940 to present) and the classification of Loeblich and Tappan (1987, 1994). Relative abundances were examined by means of principal component analysis (PCA), using SPSS (version 10.1) statistical software.

**Table 1** Age model pointers for the investigated core M-4G

| Depth (cm) | Conventional $^{14}$C age (years BP) | Calibrated $^{14}$C age (annum) | 1σ age range |
|---|---|---|---|
| 29.0–30.0 | 6,100±30 | 6,359 | 6,359–6,572 |
| 49.5–52.0 | 7,260±30 | 7,547 | 7,547–7,641 |
| 56.5–60.0 | 7,585±30 | 7,846 | 7,846–7,948 |
| 130.5–132.5 | 9,520±30 | 10,215 | 10,215–10,418 |

Additional parameters estimated are the benthic foraminifera number (BFN, i.e., number of specimens/g, which should be considered as a complex function of sedimentation rate resulting in dilution or concentration, differential taphonomic effects, and benthic production), the Shannon Wiener diversity index (H′; Magurran 1988), and the low oxygen (LO) index (Kuhnt et al. 2007, whereby high LO index values indicate low-oxygen bottom conditions). The LO index was calculated as LO=(DO*0.5)+AO, where DO is the relative abundance of dysoxic indicators (e.g., *Bolivina* spp., *Brizalina* spp., *Bulimina* spp.), and AO the relative abundance of deep infaunal species well adapted to suboxic and occasional anoxic conditions (e.g., *Cassidulinoides bradyi*, *Chilostomella mediterranensis*, *Fursenkoina* spp., *Globobulimina* spp., *Nonionella* spp.; e.g., Alavi 1988; Sen Gupta and Machain-Castillo 1993; Bernard and Sen Gupta 1999).

In all, 55 samples were used for planktonic foraminiferal analysis at a sampling interval of 1 cm (reaching 5 cm in some cases, depending on material availability), whereby at least 200 specimens were picked and identified for each sample (see Appendix B in the online electronic supplementary material). Each taxon was expressed as a percentage of the total planktonic foraminifera assemblage.

### Lipid biomarkers

In all, 108 samples were analyzed for lipid biomarkers. Lipids were extracted from freeze-dried sediments by ultrasonication using a mixture of dichloromethane/methanol (4:1, v/v), and separated into different compound classes on silica gel columns. Individual compounds were identified by gas chromatography using flame ionization detection (GC-FID) and gas chromatography coupled to mass spectrometry (GC-MS). The present study reports data on selected sterols (dinosterol), long chain alkenones (di-and triunsaturated methyl and ethyl ketones), long chain diols and keto-ols ($C_{30}$ diol and $C_{30}$ keto-ols), the isoprenoid derivatives loliolide and isololiolide, the most abundant long chain *n*-alkanols (*n*-$C_{26}$, *n*-$C_{28}$ and *n*-$C_{30}$), reported hereafter as Ter-alkanols, and the carbon preference index (CPI; Ohkouchi et al. 1997) of long chain *n*-alkanols. For more methodological information, the reader is referred to Gogou et al. (2007).

### Alkenone-based SSTs and isotope analyses

Past SSTs were estimated by means of the alkenone unsaturation index $U_{37}^{K'}$ and the global calibration given by Müller et al. (1998). Although this global calibration has been reported to perform poorly in some regional settings (e.g., Tao et al. 2012), it has been applied in the present case in order to enable comparisons with other publications dealing with Aegean sites (Gogou et al. 2007; Triantaphyllou et al. 2009a). The analytical precision based on multiple extractions of sediment samples was better than 0.6 °C.

In all, 47 samples collected every 2 cm served for isotope analyses ($\delta^{13}C$, $\delta^{18}O$) on handpicked planktonic foraminifer *Globigerina bulloides* specimens, conducted at the Stable Isotope Laboratory of the University of California, Davis. The foraminiferal tests were reacted in 105% $H_3PO_4$ at 90 °C in either an Isocarb common acid bath system or a Gilson Multicarb Autosampler system; $CO_2$ gas was analyzed in dual inlet mode on an Optima IRMS or Elementar IsoPrime, respectively. The data were computed relative to VPDB using the NBS-19 calcite standard. Precision (±1 s.d.) based on repeat analyses of an in-house calcite standard is ±0.03‰ and ±0.04‰ for $\delta^{13}C_{G.\ bulloides}$ and $\delta^{18}O_{G.\ bulloides}$, respectively.

## Results

### OC content

Higher OC values earmark sapropelic layers S1a and S1b (Fig. 3c). The maximum value of 1.94% is observed at ~9.5 ka during the deposition of S1a (minimum 0.79% at the base), whereas 1.67% is identified at 7.1 ka within S1b. The 8.0–7.7 ka interval is characterized by a reduction of OC down to 0.77% in its middle part, interpreted as the S1 interruption; an increase to 1.26% occurs at 7.6 ka, at the base of S1b (minimum 0.86% at the top).

In general, OC contents from north Aegean Sea records remain low (average of 0.5%) in the massive interval below S1; the S1i has somewhat lower OC levels (average of 1.0%) compared to the S1a and S1b layers (average of 1.9 and 1.3%, respectively), whereas the massive interval above S1 has an OC average of 0.6% (e.g., Mercone et al. 2001; Roussakis et al. 2004; Gogou et al. 2007; Katsouras et al. 2010). OC contents differ strongly between non-sapropel and sapropelic muds (>2 and <2%, respectively) in the eastern Mediterranean basins. In the case of core M-4G, the low OC is presumably the result of dilution by high terrigenous input (sedimentation rate >32 cm/1,000 years; Roussakis et al. 2004) during sapropelic formation. The sedimentation rate is high because the westward hydrodynamic regime in the area (Lykousis et al. 2002) favors high sediment influxes from the shallower Limnos Plateau (100 m depth) in the isolated depression of the core site (Fig. 1b).

### Benthic foraminifera

Benthic foraminifera are present throughout the S1 sapropelic layers, represented mostly by *Chilostomella mediterranensis*, *Globobulimina affinis*, *Cassidulinoides bradyi*, *Bolivina alata*, *B. spathulata*, *B. striatula*, *Bulimina* spp., *Uvigerina mediterranea*, *Hyalinea balthica*, *Melonis barleeanum*, agglutinants and miliolids (see Appendix A in the online electronic supplementary material; Fig. 4). All specimens are very well preserved without pyrite infillings having been observed, indicating in situ deposition as supported also by the lithologic-sedimentary features of the core M-4G sequence. Shallow water species such as *Ammonia beccarii*, *Elphidium* spp. and *Rosalina* spp. contribute less than 1% to the assemblages. Agglutinants and miliolids occur in very low to zero levels within S1, but increase significantly outside the sapropelic interval and during the sapropel interruption. *C. mediterranensis* is found in both S1 lobes, reaching almost 30% at ~9.1 ka and 25% at 6.8 ka. *G. affinis* exceeds 70% at ~9.6 ka (S1a), but is almost absent after 8.0 ka. *C. bradyi* shows a similar pattern, with much lower abundance (up to 5% at 9.9 ka). *B. alata* fluctuates during S1 deposition, peaking at ~7.3 ka. *B. spathulata* displays low values during S1a; the highest abundance (30%) is observed at ~7.6 ka (S1b). *B. striatula* peaks at 8.2 ka (up to 13%) and during the deposition of S1b. *Bulimina* spp. (mainly *B. marginata*, *B. striata*) represent a significant component (up to 40%, particularly within S1a), with an increasing trend between 9.6–8.5 ka. *U. mediterranea* reaches up to ~24% at about 10.1 ka (base of S1a), and a gradual decrease is observed in S1i; values also increase during S1b. *H. balthica* increases strongly within S1b, to reach a maximum of ~17% at 7.0 ka. Higher values of *M. barleeanum* are observed at the bottom of S1a, toward the top of S1b, and outside the sapropelic interval.

The LO index rises gradually within S1a to reach 80 at ~9.6 ka (Fig. 5); the S1i features an average value of 33, whereas the LO index reaches 40 within S1b. The H′ index is characterized by a prominent decrease (value close to 1.0) in the period 9.8–9.6 ka during S1a deposition. No major change is observed within the S1i and S1b intervals, with values close to 2.4; such moderate values are quite normal in oligotrophic Mediterranean ecosystems and in well-oxygenated eutrophic waters (Fontanier et al. 2014). The total number of benthic foraminifera (BFN) is low throughout the S1 sapropelic layers, and generally high in non-sapropelic deposits (Fig. 5).

In the PCA results (Fig. 5, Table 2), the PC1 component accounts for 56% of the total variance, and shifts to a negative range in the lower interval of S1; positive values characterize the S1i. PC1 represents relatively high oxygen concentrations, as it is positively loaded by total agglutinated species (0.95), *Bulimina aculeata* (0.91), and *U. mediterranea* (0.91) characteristic of well-oxygenated bottom conditions (e.g., Alve 1995). PC2, having positive values except for the ~10.2–9.2 ka interval, explains a further 11% of the variance and is positively loaded (0.64) mainly by the occasionally labile OM-feeding *C. mediterranensis* (e.g., Fontanier et al. 2002; Kuhnt et al. 2007).

## Planktonic foraminifera

Planktonic foraminifera assemblages are composed of *Globigerinoides ruber* (var. *alba* and *rosea*), *G. sacculifer*, *G. conglobatus*, *Globoturborotalita rubescens*, *Orbulina universa*, *Globigerinella siphonifera*, *G. calida*, *Globigerina bulloides*, *G. falconensis*, *Turborotalita quinqueloba*, *Globorotalia inflata*, *G. crassaformis*, *G. scitula*, *Globigerinita glutinata*, *Neogloboquadrina pachyderma* (dextral), and *N. dutertrei*. The downcore variations of the most abundant species are presented in Fig. 6 (also see Appendix B in the online electronic supplementary material).

Among the abovementioned species, *G. siphonifera*, *G. rubescens*, *O. universa*, *G. sacculifer* and *G. calida*, which belong to the SPRUDTS group (Rohling et al. 1993), and *G. ruber* (var. *alba* and *rosea*) dominate warm and oligotrophic summer mixed layers in subtropical regions, including the eastern Mediterranean (Pujol and Vergnaud Grazzini 1995; Rohling et al. 2002a). Therefore, the downcore variation of the sum of their percentages (warm planktonic foraminifera curve, WPFC) is considered as an indicator of SST variability (Fig. 6). WPFC variations are similar to those in the corresponding $\delta^{18}O$ record (see below), with lower values at 9.7–8.8 and 8.2 ka within the S1a layer and at 7.4, 7.0 and 6.8 ka during the deposition of S1b.

*T. quinqueloba* and *G. bulloides* are the dominant species, reaching 75% and 45%, respectively. *G. bulloides* abundance, although fluctuating, is more pronounced at 9.7–9.2 ka, as well as at 8.8–8.3, 7.7–8.0, and 6.8–7.0 ka. *T. quinqueloba* increases at 10.0–9.0 ka (base of S1a), 8.4–8.0 ka (top of S1a), and 7.0–6.5 ka (top of S1b). *G. inflata* and Neogloboquadrinids (sum of *N. pachyderma* (dextral) and *N. dutertrei*) reach relative percentages of 12% and 13%, respectively at 8.0–7.3 ka. Furthermore, the proportion of *G. inflata* is high at 6.7–6.0 ka (i.e., end of S1 deposition), and that of Neogloboquadrinid species at 7.0–6.6 ka. The downcore variation of the sum of the percentages of the abovementioned species (*G. bulloides*, *T. quinqueloba*, *N. dutertrei*, *N. pachyderma* (dextral), *G. inflata*) is presented in Fig. 6 as "eutrophic species".

## Lipid biomarkers

Contents (ng/g of sediment dry weight) of lipid biomarkers and CPI values for *n*-alkanols are presented in Fig. 7. Ter-alkanols exhibit higher abundance in the S1a interval compared to S1b (average of 594 and 347 ng/g, respectively), with maximum values recorded at 9.5 ka. The average CPI values of high molecular *n*-alkanols range between 6.65 and 11.92. CPI values start to increase at ~7.7 ka, exhibiting sequential peaks within the S1b interval that represent the highest values of the entire record (Fig. 7). A series of marine lipid biomarkers of algal origin ($C_{37:2}$ alkenone, $C_{30}$ diols and keto-ols, dinosterol, loliolide and isololiolide) is also present in all samples, exhibiting similar distributions with higher abundances recorded during S1a deposition in comparison to S1b; a remarkable

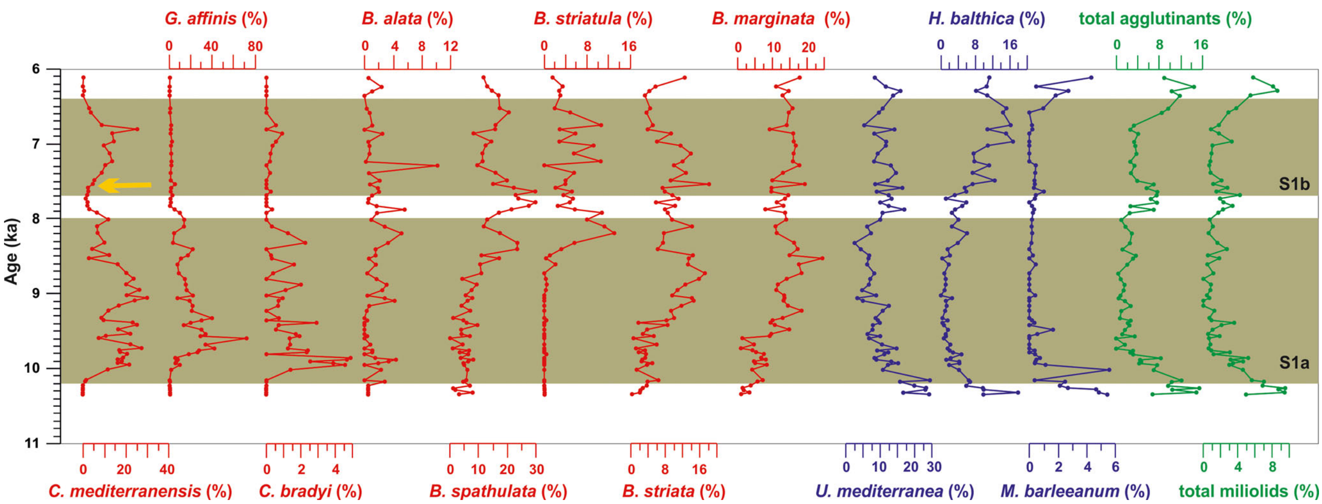


**Fig. 4** Relative abundances (%) of the main benthic foraminiferal species of core M-4G. *Yellow arrow* Increase of labile OM-feeding *C. mediterranensis* after ~7.5 ka. *Shaded areas* Periods of deposition of S1a and S1b layers

incremental trend is evident at 7.5–6.5 ka (S1b). Long chain alkenones are present in all samples, with $C_{37:2}$ predominating; values increase within S1a at ~9.8 ka, exceeding 300 ng/g at ~9.3 ka, and are prominently lower in S1b (Fig. 7). $C_{30}$ diol and keto-ols, the isoprenoid derivatives loliolide and isololiolide, and dinosterol display similar trends. Lipid biomarkers are essentially absent in the S1i interval.

### $U_{37}^{K'}$ SSTs, $\delta^{18}O_{G.\ bulloides}$, $\delta^{13}C_{G.\ bulloides}$

Alkenone-based SSTs show a general warming trend with shorter-term fluctuations throughout S1 (Fig. 8a), reaching 20.6 °C at the beginning of S1a deposition (9.8 ka) and 20.2 °C at ~8.5 ka. Marked drops in SST are observed at 9.5, 9.3, 8.6, and ~8.2 ka; two pronounced coolings are centered at 7.8 and 7.4 ka, during the S1i and within S1b. In general, SSTs are higher in the period ~9.0–8.0 ka (average 19.8 °C) compared to the lower part of S1a (average18.9 °C). S1b is characterized by values (average 18.8 °C) similar to those of S1a (average 19.2 °C).

Despite the $\delta^{18}O$ and $\delta^{13}C$ records being relatively low in resolution, it is possible to observe a shift to larger isotopic values in the $\delta^{18}O_{G.\ bulloides}$ record at 8.6 ka, the signatures varying between 0.32 and 1.88‰. A series of fluctuations within S1b is also evident in the $\delta^{18}O_{G.\ bulloides}$ record, with

**Fig. 5** **a** Low oxygen (LO) index, **b** benthic foraminiferal (BF) diversity (H′), **c** total number of benthic foraminifera (BFN), **d**, **e** PCA components. *Shaded areas* Periods of deposition of S1a and S1b layers

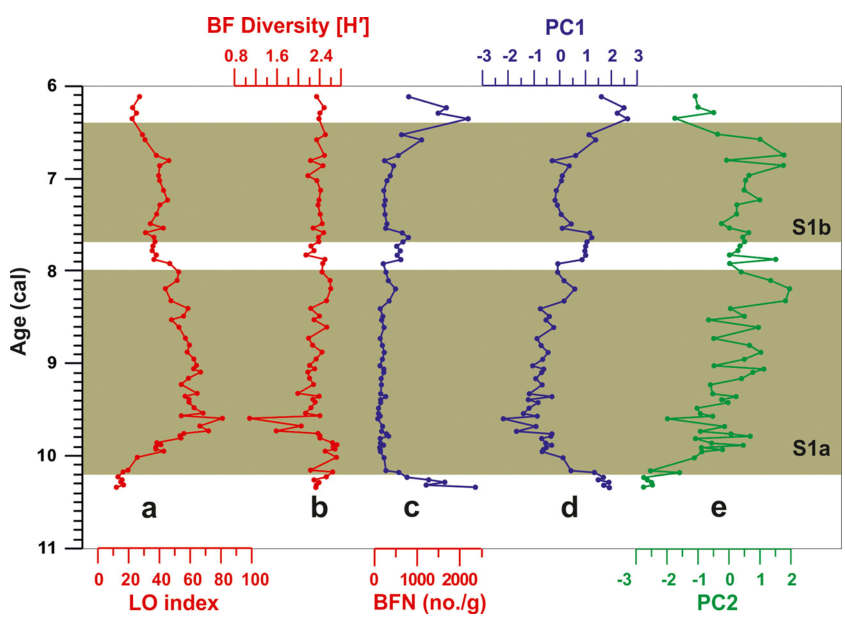

**Table 2** Factor loadings of benthic foraminifera taxa on the first two principal component axes. The significant loadings are shown in italics

| Component matrix | Component | |
|---|---|---|
| | 1 | 2 |
| *Bolivina spathulata* | 0.90 | 0.30 |
| *Bolivina striatula* | 0.69 | 0.45 |
| *Bolivina alata* | 0.58 | 0.48 |
| *Bulimina marginata* | 0.84 | 0.32 |
| *Bulimina costata* | 0.76 | 0.38 |
| *Bulimina aculeate* | *0.91* | –0.12 |
| *Globobulimina affinis* | –0.74 | 0.33 |
| *Uvigerina mediterranea* | *0.91* | –0.11 |
| *Hanzawaia boueana* | 0.70 | 0.28 |
| *Hyalinea balthica* | 0.88 | 0.11 |
| *Melonis pompilioides* | 0.74 | –0.40 |
| *Cassidulina crassa* | 0.68 | –0.08 |
| *Globocassidulina subglobosa* | 0.75 | –0.12 |
| *Nonionella turgida* | –0.18 | 0.52 |
| *Cassidulinoides bradyi* | –0.37 | 0.34 |
| Miliolids | 0.88 | –0.22 |
| Agglutinants | *0.95* | –0.05 |
| *Chilostomella mediterranensis* | –0.55 | *0.64* |

a prominent shift to larger values at 7.4 ka (Fig. 8c). The $\delta^{13}C_{G.\ bulloides}$ pattern ranges between –2.37 and –1.26‰, and exhibits a trend toward more negative values after 9.0 ka, except for the S1i interval. A prominent $\delta^{13}C$ increase is recorded at ~7.0 ka (Fig. 8b).

## Discussion

The data reported above enable the reconstruction of paleoceanographic-paleoclimatic conditions during the Holocene Climatic Optimum in the south Limnos Basin. Thereby, three main phases can be distinguished.

### 10.2–8.0 ka (S1a sapropelic layer)

During the ~10.2–9.0 ka interval, S1a is characterized (Fig. 4) by the high abundance of benthic foraminiferal species able to tolerate surface sediment and/or pore water oxygen depletion, such as *C. mediterranensis*, *G. affinis*, *B. striata* and *C. bradyi* (e.g., Bernard and Sen Gupta 1999; Fontanier et al. 2002, 2008a, 2008b, 2014; Kuhnt et al. 2007; Abu-Zied et al. 2008), and the presence of *U. mediterranea*, which thrives in oxic mesotrophic to eutrophic environments (e.g., Jorissen et al. 1995; Schmiedl et al. 2000). Hence, benthic foraminiferal data combined with highest values of the LO index, lowest benthic diversity, and the PC1 component pattern at 9.8–9.6 ka (Fig. 5) indicate dysoxic to oxic bottom waters and preservation of organic matter (cf. high OC contents as well as loliolide and isololiolide values; Figs. 3c, 7). The positive shifts in OC also reflect the enhanced marine algal productivity that is evident in the biomarkers records, which all exhibit maxima between 9.8–9.0 ka (Fig. 7). This is well correlated with the dominance of eutrophic planktonic foraminifera species, particularly with the commonly nutrient-dependent *G. bulloides* (9.7–9.2 ka, Fig. 6; e.g., Schiebel et al. 2004). High percentages of this taxon have been reported in the

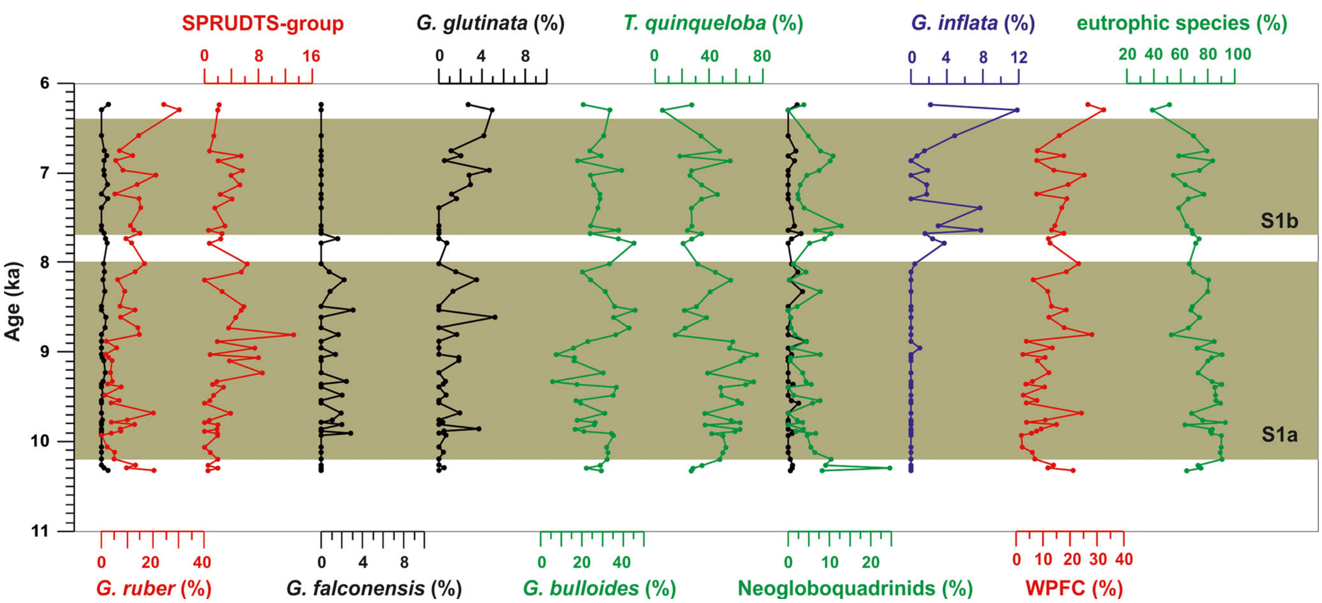


**Fig. 6** Relative abundances (%) of planktonic foraminifera species of core M-4G. In the diagrams of *G. ruber* and Neogloboquadrinids: *black* abundances of *G. ruber* (*rosea*) and *N. dutertrei*; *red and green* abundances of *G. ruber* (*alba*) and *N. pachyderma* (dextral), respectively. SPRUDTS group (Rohling et al. 1993): percentages of *G. siphonifera*, *G. rubescens*, *O. universa*, *G. sacculifer*, and *G. calida*. *WPFC* Warm planktonic foraminifera curve; *shaded areas* periods of deposition of S1a and S1b layers

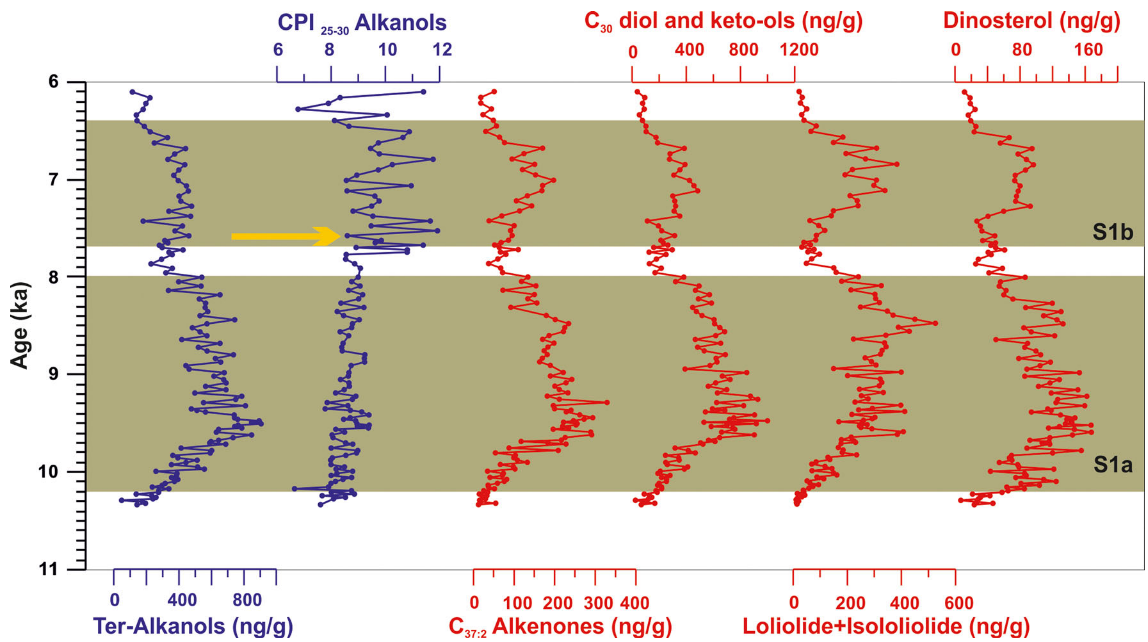


**Fig. 7** Contents (ng/g) of investigated lipid biomarkers. *Yellow arrow* Delivery of less degraded terrestrial organic matter in the south Limnos Basin after ~7.8 ka and through to the end of S1b deposition. *Shaded areas* Periods of deposition of S1a and S1b layers

sediments of S1 in the Aegean Sea, mainly in the north (Zachariasse et al. 1997; Geraga et al. 2010) rather than in the south basins (e.g., Geraga et al. 2000; Casford et al. 2002; Triantaphyllou et al. 2009b), reflecting the higher riverine/nutrient input into the north Aegean during the early Holocene (e.g., Gogou et al. 2007; Kotthoff et al. 2008; Triantaphyllou 2014).

In the ~10.0–9.0 ka time interval, the $U_{37}^{K'}$ SST values (Fig. 8a) imply surface water temperature increase, interestingly featuring somewhat lower values compared with the upper part of S1a (9.0–8.0 ka). In contrast, WPFC values are conspicuously low, partly masked by the prevalence of fresher surface waters occurring at that time, as shown by the high abundance of *T. quinqueloba* (Fig. 6). *T. quinqueloba* has been recorded to exhibit opportunistic behavior in response to nutrient-rich, low-salinity, and low-turbidity river discharge into warm oligotrophic stratified marine waters (e.g., Retailleau et al. 2012). Hence, the shifts to smaller values observed in the $\delta^{18}O_{G.\ bulloides}$ record can be indicative of salinity lowering rather than temperature increase, as they are negatively correlated with the alkenone-based SST curve (Fig. 8a, c); $\delta^{18}O_{G.\ bulloides}$ has been used to estimate the Mediterranean surface salinity pattern associated with the last sapropel (e.g., Kallel et al. 1997). Apparently, the potential lowering of salinity between 10.0 and 9.0 ka can be attributed to high riverine input into the north Aegean basins and/or higher precipitation rates (e.g., Aksu et al. 1999; Casford et al. 2002; Kotthoff et al. 2008; Kuhnt et al. 2008). This interpretation is also supported by the concurrent increase in Ter-alkanols (Fig. 7), indicating frequent pulses of terrigenous OM (e.g., Gogou et al. 2007; Meyers and Arnaboldi 2008; Katsouras et al. 2010), and by the high prevalence of *T. quinqueloba* (see above).

During the last millennium of S1a deposition (9.0–8.0 ka) and particularly at ~8.2 ka, the benthic assemblages display decreases of species indicative of oxygen depletion, along with increments of *B. spathulata*, *B. striatula* and *B. alata*, i.e., species relatively tolerant to low-oxygen conditions (e.g., Jorissen et al. 1995; Alve and Murray 1999). *H. balthica*, an opportunistic taxon responding positively to high food availability (Rosenthal et al. 2011), rises after 8.5 ka (Fig. 4). The benthic foraminiferal data imply weaker bottom water dysoxia in the north Aegean/south Limnos basins at 9.0–8.0 ka, compared to the early stages of S1a. Within the same time interval, increased abundance of *G. bulloides*, higher $\delta^{13}C_{G.\ bulloides}$ values, and positive shifts in marine algal biomarkers (Figs. 6, 7, 8b) suggest enhanced productivity in the water column. The associated lower SSTs at ~8.2 ka (Fig. 8a) add evidence to an abrupt SST minimum related to the cold "8.2 ka" event (Rohling and Pälike 2005; Marino et al. 2009; Rohling et al. 2015).

## 8.0–7.7 ka (interruption of sapropelic deposition)

The recorded interruption of S1 at ~8.0 ka in the south Limnos Basin M4-G core features cooler conditions in the water column as indicated by alkenone-based SSTs (minimum at 7.8 ka; Fig. 8a), and the shift of $\delta O^{18}_{G.\ bulloides}$ records toward larger values (Fig. 8c); the latter could also be related to freshwater inflow. The interruption within sapropel S1 in the north Aegean (~8.4–7.9 ka; Kotthoff et al. 2008) displays a peak in freshwater input together with decrease in stratification and

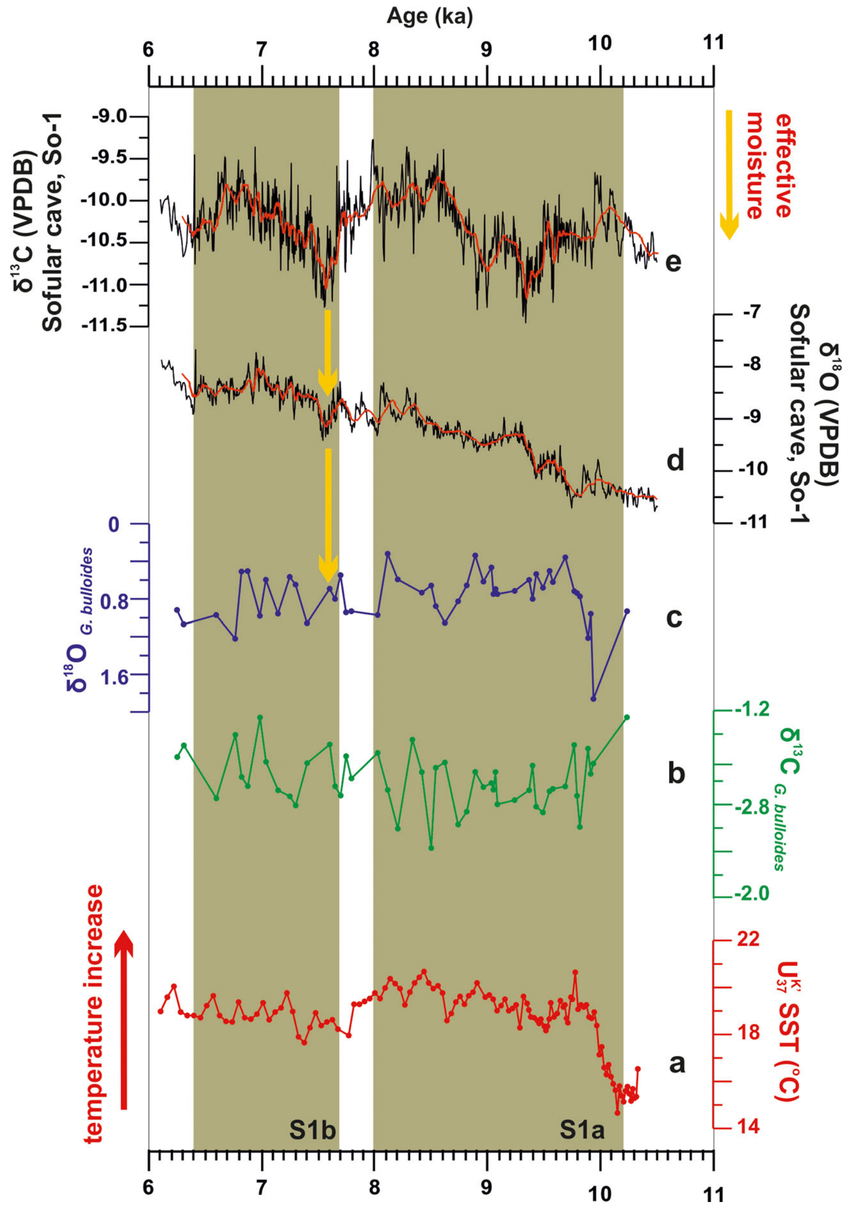


**Fig. 8** Northeastern Aegean and southern Black Sea coast comparison (Sofular Cave). **a** $U^{K'}_{37}$ SST values for core M-4G. **b**, **c** M-4G $\delta^{13}C_{G.\ bulloides}$ and $\delta^{18}O_{G.\ bulloides}$ patterns. **d**, **e** Sofular Cave $\delta^{18}O$ and $\delta^{13}C$ patterns (*black* raw data, *red* 19-point running average). *Yellow arrows* Increase in effective moisture along the southern Black Sea coast at ~7.5 ka, accompanied by reduced salinity and increase of labile organic matter in the NE Aegean (see Figs. 4, 7). *Shaded areas* Periods of deposition of S1a and S1b layers

relevant deep water formation under the influence of cold and dry polar/continental air masses from higher latitudes (Triantaphyllou 2014).

OC values in the S1i are low, similarly to those recorded at the base and top of the S1 layers in core M-4G (Fig. 3c). The interruption interval is earmarked by a peak of *U. mediterranea* and decreasing patterns of benthic foraminifera species tolerant to oxygen depletion (Fig. 4). The accompanying decline in marine organic markers (Fig. 7) and the LO index (Fig. 5) indicates lower preservation due to higher bottom oxygen levels. Furthermore, the increases of the deep dwellers *G. inflata*, Neogloboquadrinids and *G. bulloides* linked to relatively cold temperatures and food supply (Fig. 6) suggest high primary production and stronger mixing of the water column at least during the winter season (e.g., Pujol and Vergnaud Grazzini 1995; Casford et al. 2002; Schiebel et al. 2004; Rigual-Hernández et al. 2012).

### 7.7–6.4 ka (S1b sapropelic layer)

The foraminiferal records, particularly the impressively reduced deep infaunal species (Fig. 4), imply rather oxic conditions at the M-4G core site during the S1b interval when compared to other Aegean sites (e.g., Aksu et al. 2002; Geraga et al. 2005, 2010; Kuhnt et al. 2007; Abu-Zied et al. 2008; Triantaphyllou et al. 2009a; Schmiedl et al. 2010). In particular, the relatively high BFN values after 7.0 ka (Fig. 5), combined with the lower LO index and OC content (Figs. 3, 5), rise of the benthic species *U. mediterranea* and *H. balthica*, absence of *G. affinis*, moderate abundance of

*C. mediterranensis* (exceeding 20% only at ~6.7 ka; Fig. 4), increased contribution of *G. bulloides* and Neogloboquadrinids (Fig. 6), and prominent shift of the $\delta^{13}C_{G.\ bulloides}$ record to less negative values at 7.0 ka (Fig. 8b) all suggest eutrophic conditions, higher oxygen levels, and labile food sources. More oxic bottom waters are also well expressed in the distribution of PC1 and PC2 components (Fig. 5); interestingly, PC2 is well correlated with the downcore variation of the eutrophic planktonic species abundance (Fig. 6), pointing to surface water productivity.

S1b is characterized by slightly lower, albeit strongly fluctuating SSTs compared to S1a (prominent minimum at 7.4 ka; Fig. 8a), together with a series of concomitant positive shifts in the $\delta^{18}O_{G.\ bulloides}$ record (Fig. 8c). *U. mediterranea* increases at 7.4, 7.0, 6.8, and ~6.5 ka (Fig. 4) are associated with conspicuous SST minima (Fig. 8a), imprinting repeated cold outbursts in the north Aegean during the late HCO. *U. mediterranea* is commonly adapted to moderate or high fluxes of labile OM in combination with well-ventilated bottom waters, and has proven to increase in the final stage or subsequently after cold events (e.g., Schmiedl et al. 2000; Kuhnt et al. 2007). Apparently, there is a straightforward correlation of the rapid coolings in S1b with associated occurrence of dense water formation events (e.g., Schmiedl et al. 2010), which are notably amplified in the M-4G high-resolution record due to the shallow depositional depth.

### Inferred freshwater sources

The increased contribution of Ter-alkanols during S1a in the M-4G sediment record (Fig. 7) points to enhanced riverine inputs and/or intense rainfalls (Kotthoff et al. 2008), in accordance with the slightly smaller $\delta^{18}O_{G.\ bulloides}$ values recorded in the same interval (Fig. 8c). Inflow of low-salinity surface waters in the north Aegean during S1a is supported by the findings of Triantaphyllou (2014), who reported evidence of a strongly stratified water column at a neighboring core site (core SL-152, Athos Basin).

Ter-alkanols are considerably lower within S1b (Fig. 7), suggesting weaker supply of terrigenous input related either with slower sedimentation rate or with increase in distance from the surrounding river mouths due to the rise in north Aegean sea level from –40 m at 10.0 ka to –5 m at 6.0 ka (Pavlopoulos et al. 2012, 2013), and/or lower preservation as a result of more oxic bottom conditions. In addition, there is a marked shift of the *n*-alkanols CPI to higher values from S1a to S1b (8.66±0.41 for S1a, and 9.74±0.98 for S1b; Fig. 7). The CPI of long chain *n*-alkanols (typically >4) has been used as an indicator of terrestrial OM degradation (e.g., Collister et al. 1994; Ohkouchi et al. 1997). High CPI values have been found in north Aegean sediments for the last 2.0 thousand years (average 7.0; Gogou et al., unpublished data), and the Black Sea (>9.5 in modern sinking particulate matter; Parinos and Gogou, unpublished data). Indeed, present-day BSW transfers important loadings of dissolved and particulate organic carbon to the north Aegean Sea (Frangoulis et al. 2010; Meador et al. 2010; Lagaria et al. 2013). Thus, a shift to higher CPI values indicates the delivery of fresher (less degraded) terrestrial OM in the south Limnos Basin after ~7.7 ka and through to the end of S1b.

Interestingly, OC contents display slight increases (Fig. 3c) and all algal biomarkers exhibit positive shifts between 7.5 and 6.6 ka (Fig. 7), pinpointing an enhanced in situ productivity and preservation of labile marine OM. This fits well with concomitant increases of the labile OM-feeding benthic foraminifer *U. mediterranea* (e.g., Schmiedl et al. 2000; Kuhnt et al. 2007), the occasionally labile OM-feeding *C. mediterranensis* (e.g., Fontanier et al. 2002, 2005; Kuhnt et al. 2007), and the eutrophic planktonic species *G. bulloides* (e.g., Rohling et al. 1997).

Consequently, the higher contributions of labile marine OM along with fresher terrestrial OM inputs after ~7.7 ka imply sources alternative/ additional to the north Aegean borderland riverine sources for the influx of organic matter in the south Limnos Basin. The more efficient vertical convection caused by repeated dense water formation events at a centennial scale, with major cooling at 7.4 ka followed by cold spells at 7.0, 6.8, and 6.5 ka (see above), offered an additional forcing for the subsequent increase of in situ primary production.

The robust chronological framework built for the M-4G sediment record can be correlated with climate signals from the highly resolved Sofular Cave speleothem along the southern Black Sea coast (Fleitmann et al. 2009; Goktürk et al. 2011). Both $\delta^{18}O$ and $\delta^{13}C$ Sofular Cave curves comprise distinct peaks of more negative values and subsequent wetter conditions centered at ~7.5 ka (Fig. 8d, e). Bearing in mind that a significant outflow of Black Sea water into the Sea of Marmara started at ~9.0 ka due to an increase in regional precipitation (e.g., Sperling et al. 2003; Vidal et al. 2010), it is reasonable that the highly productive Marmara Sea/Black Sea waters contributed to the labile OM influx at the M-4G core site. Obviously, the well-documented precipitation/ effective moisture increase in the southern Black Sea affected the Marmara/BSW inflow in the NE Aegean, plausibly causing the *n*-alkanols CPI shift to higher values during S1b formation (Fig. 7), and increases in the abundance of labile OM-feeding benthic foraminifers and eutrophic planktonic species (Figs. 4, 6) after 7.7 ka at the M-4G core site.

## Conclusions

In the shallow south Limnos Basin of the NE Aegean Sea, the early stage of the Holocene Climatic Optimum is marked by the deposition of the S1a sapropelic interval. Particularly in its lower part dated ~10.2 to 9.0 ka, the S1a layer is characterized by dysoxic to oxic bottom waters, as revealed by the predominance of benthic foraminiferal species tolerant to oxygen depletion (*C. mediterranensis*, *G. affinis*, *B. striata*, *B. marginata*) together with the oxic mesotrophic-eutrophic dweller *U. mediterranea.* Preservation of OM is evidenced by the high OC as well as loliolide and isololiolide contents, while enhanced marine algal productivity is clearly seen in the biomarker record and the abundances of eutrophic planktonic foraminifera. The surface waters feature somewhat lower SSTs (average 18.9 °C) compared to the upper part of S1a (9.0–8.0 ka; average 19.8 °C). The increase in Ter-alkanols during the same interval is associated with frequent pulses of terrigenous OM; accordingly, the $\delta^{18}O_{G.\ bulloides}$ record exhibits a shift to smaller values, suggesting salinity decrease that can be attributed to riverine input from the north Aegean borderland. Cooling is indicated by both alkenone-based SSTs and $\delta O^{18}_{G.\ bulloides}$ records at 8.2 ka and during the S1 interruption at ~7.8 ka.

Within the late stage of the HCO, the sapropelic layer S1b (7.7–6.4 ka) is characterized by rather oxic conditions; the contribution of foraminiferal species tolerant to oxygen depletion is very low, in contrast to the abundance of the benthic foraminifer *U. mediterranea* common in oxic mesotrophic-eutrophic environments. Strongly fluctuating alkenone-based SSTs denote paleoclimatic instability and associated occurrence of dense water formation events on a centennial scale, with major cooling at 7.4 ka, followed by cold spells at 7.0, 6.8, and 6.5 ka. Weaker terrigenous influx is reflected in the considerably lower Ter-alkanols values; however, the prominent rise of the CPI index indicates the delivery of less degraded terrestrial OM. The increase of algal biomarkers, labile OM-feeding foraminifera (*C. mediterranensis*, *U. mediterranea*) and eutrophic planktonic species pinpoints a rise in marine productivity, which is reinforced by more efficient vertical convection due to repeated dense water formation events. Higher contributions of labile marine OM along with less degraded terrestrial OM inputs after ~7.7 ka imply sources alternative/additional to the north Aegean borderland riverine sources in the south Limnos Basin, plausibly related to the inflow of highly productive Marmara/Black Sea waters.

**Acknowledgements** This work was financially supported by the EU Marine ERA/MedEcos and EU/FP7 Perseus projects. We acknowledge constructive assessments by E. Malinverno and the journal editors.

Conflict of interest: The authors declare that there is no conflict of interest with third parties.

## References

Abu-Zied RH, Rohling E, Jorissen FJ, Fontanier C, Casford JSL, Cooke S (2008) Benthic foraminiferal response to changes in bottom-water oxygenation and organic carbon flux in the eastern Mediterranean during LGM to Recent times. Mar Micropaleontol 67:46–68

Aksu AE, Yaşar D, Mudie PJ, Gillespie H (1995) Late glacial-Holocene paleoclimatic and paleoceanographic evolution of the Aegean Sea: micropaleontological and stable isotopic evidence. Mar Micropaleontol 25:1–28

Aksu AE, Abrajano T, Mudie PJ, Yaşar D (1999) Organic geochemical and palynological evidence for terrigenous origin of the organic matter in Aegean Sea sapropel S1. Mar Geol 153:303–318

Aksu AE, Hiscott RN, Mudie PJ, Rochon A, Kaminski MA, Abrajano T, Yaşar D (2002) Persistent Holocene outflow from the Black Sea to the Eastern Mediterranean contradicts Noah's Flood hypothesis. GSA Today 12:4–10

Alavi SN (1988) Late Holocene deep-sea benthic foraminifera from the Sea of Marmara. Mar Micropaleontol 13:213–237

Alley RB, Mayewski PA, Sowers T, Stuiver M, Taylor KC, Clark PU (1997) Holocene climatic instability: a prominent, widespread event 8200 yr ago. Geology 25:483–486

Alve E (1995) Benthic foraminifera response to estuarine pollution: a review. J Foram Res 25:190–203

Alve E, Murray JW (1999) Marginal marine environments of the Skagerrak and Kattegat: a baseline study of living (stained) benthic foraminiferal ecology. Palaeogeogr Palaeoclimatol Palaeoecol 146: 171–193

Bahr A, Arz HW, Lamy F, Wefer G (2006) Late glacial to Holocene paleoenvironmental evolution of the Black Sea, reconstructed with stable oxygen isotope records obtained on ostracod shells. Earth Planet Sci Lett 241:863–875

Bernard JM, Sen Gupta BK (1999) Foraminifera of oxygen-depleted environments. In: Sen Gupta BK (ed) Modern Foraminifera. Kluwer, Dordrecht, pp 201–216

Casford JSL, Rohling EJ, Abu-Zied R, Cooke S, Fontanier C, Leng M, Lykousis V (2002) Circulation changes and nutrient concentrations in the late Quaternary Aegean Sea: a nonsteady state concept for sapropel formation. Paleoceanography 17:1024–1034

Casford JSL, Rohling EJ, Abu-Zied RH, Fontanier C, Jorissen FJ, Leng MJ, Schmiedl G, Thomson J (2003) A dynamic concept for eastern Mediterranean circulation and oxygenation during sapropel formation. Palaeogeogr Palaeoclimatol Palaeoecol 190:103–119

Casford JSL, Abu-Zied R, Rohling EJ, Cooke S, Fontanier C, Leng M, Millard A, Thomson J (2007) A stratigraphically controlled multiproxy chronostratigraphy for the eastern Mediterranean. Paleoceanography 22(4), PA4215. doi:10.1029/2007PA001422

Collister JW, Rieley G, Stern B, Eglinton G, Fry B (1994) Compound-specific $\delta^{13}C$ analyses of leaf lipids from plants with differing carbon dioxide metabolisms. Org Geochem 21:619–627

De Lange GJ, Thomson J, Reitz A, Slomp CP, Principato MS, Erba E, Corselli C (2008) Synchronous basin-wide formation and redox-controlled preservation of a Mediterranean sapropel. Nature Geosci 1:606–610

Duchemin G, Fontanier C, Jorissen FJ, Barras C, Griveaud C (2007) Living small-sized (63–150 mm) foraminifera from mid-shelf to mid-slope environments in the Bay of Biscay. J Foram Res 37:12–32

Ellis BF, Messina A (1940 to present) Catalogue of Foraminifera. Special publication, The American Museum of Natural History, New York

Facorellis Y, Maniatis Y, Kromer B (1998) Apparent $^{14}C$ ages of marine mollusk shells from a Greek island: calculation of the marine reservoir effect in the Aegean Sea. Radiocarbon 40:963–973

Fleitmann D, Cheng H, Badertscher S, Edwards RL, Mudelsee M, Göktürk OM, Fankhauser A, Pickering R, Raible CC, Matter A, Kramers J, Tuysuz O (2009) Timing and climatic impact of Greenland interstadials recorded in stalagmites from northern Turkey. Geophys Res Lett 36, L19707. doi:10.1029/2009GL040050

Fontanier C, Jorissen FJ, Licari L, Alexandre P, Anschutz P, Carbonel P (2002) Live benthic foraminiferal faunas from the Bay of Biscay:

faunal density, composition, and microhabitats. Deep-Sea Res I 49: 751–785

Fontanier C, Jorissen FJ, Chaillou G, Anschutz P, Grémare A, Griveaud C (2005) Live foraminiferal faunas from a 2800 m deep lower canyon station from the Bay of Biscay: faunal response to focusing of refractory organic matter. Deep-Sea Res I 52:1189–1227

Fontanier C, Jorissen FJ, Geslin E, Zaragosi S, Duchemin G, Laversin M, Gaultier M (2008a) Live and dead foraminiferal faunas from the Saint-Tropez Canyon (Bay of Fréjus): observations based on in situ and incubated cores. J Foram Res 38:137–156

Fontanier C, Jorissen FJ, Lansard B, Mouret A, Buscail R, Schmidt S, Kerhervé P, Buron F, Zaragosi S, Hunault G, Ernoult E, Artero C, Anschutz P, Rabouille C (2008b) Live (stained) foraminiferal faunas from open slope environments separating submarine canyons in the Gulf of Lions (NW Mediterranean): diversity, density and microhabitats. Deep-Sea Res I 55:1532–1553

Fontanier C, Koho KA, Goñi-Urriza MS, Deflandre B, Galaup S, Ivanovsky A, Gayet N, Dennielou B, Grémare A, Bichon S, Gassie C, Anschutz P, Duran R, Reichart GJ (2014) Benthic foraminifera from the deep-water Niger delta (Gulf of Guinea): assessing present-day and past activity of hydrate pockmarks. Deep-Sea Res I 94:87–106

Frangoulis C, Psarra S, Zervakis V, Meador T, Mara P, Gogou A, Zervoudaki S, Giannakourou A, Pitta P, Lagaria A, Krasakopoulou E, Sioukou-Frangou I (2010) Connecting export fluxes to plankton food-web efficiency in the Black Sea waters inflowing into the Mediterranean Sea. J Plankt Res 32:1203–1216

Geraga M, Tsaila-Monopolis S, Ioakim C, Papatheodorou G, Ferentinos G (2000) An evaluation of paleoenvironmental changes during the last 18000 yr BP in the Myrtoon Basin, S.W. Aegean Sea. Palaeogeogr Palaeoclimatol Palaeoecol 156:1–17

Geraga M, Tsaila-Monopolis S, Ioakim C, Papatheodorou G, Ferentinos G (2005) Short-term climate changes in the southern Aegean Sea over the last 48,000 years. Palaeogeogr Palaeoclimatol Palaeoecol 220:311–332

Geraga M, Ioakim C, Lykousis V, Tsaila-Monopolis S, Mylona G (2010) The high resolution palaeoclimatic and palaeoceanographic history of the last 24,000 years in the central Aegean Sea, Greece. Palaeogeogr Palaeoclimatol Palaeoecol 287:101–115

Gogou A, Bouloubassi I, Lykousis V, Arnaboldi M, Gaitani P, Meyers PA (2007) Organic geochemical evidence of abrupt late glacial-Holocene climate changes in the North Aegean Sea. Palaeogeogr Palaeoclimatol Palaeoecol 256:1–20

Goktürk OM, Fleitmann D, Badertscher S, Cheng H, Edwards RL, Leuenberger M, Fankhauser A, Tüysüz O, Kramers J (2011) Climate on the southern Black Sea coast during the Holocene: implications from the Sofular Cave record. Quat Sci Rev 30:2433–2445

Grimm R, Maier-Reimer E, Mikolajewicz U, Schmiedl G, Müller-Navarra K, Adloff F, Grant KM, Ziegler M, Lourens LJ, Emeis K-C (2015) Late glacial initiation of Holocene eastern Mediterranean sapropel formation. Nature Commun 6:7099. doi:10.1038/ncomms8099

Hiscott RN, Aksu AE, Mudie PJ, Marret F, Abrajano T, Kaminski MA, Evans J, Çakiroglu AI, Yasar D (2007) A gradual drowning of the southwestern Black Sea shelf: evidence for a progressive rather than abrupt Holocene reconnection with the eastern Mediterranean Sea through the Marmara Sea Gateway. Quat Int 167–168:19–34

Jorissen FJ, Barmawidjaja DM, Puskaric S, Van der Zwaan GJ (1992) Vertical distribution of benthic Foraminifera in the Northern Adriatic Sea. The relation with high organic flux. Mar Micropaleontol 19: 131–146

Jorissen FJ, De Stigter HC, Widmark JGV (1995) A conceptual model explaining benthic foraminiferal microhabitats. Mar Micropaleontol 26:3–15

Kallel N, Paterne M, Duplessy JC, Vergnaud-Grazzini C, Pujol C, Labeyrie LD, Arnold M, Fontugne M, Pierre C (1997) Enhanced rainfall in the Mediterranean region during the last sapropel event. Oceanol Acta 20:697–712

Katsouras G, Gogou A, Bouloubassi I, Emeis KC, Triantaphyllou M, Roussakis G, Lykousis V (2010) Organic carbon distribution and isotopic composition in three records from the eastern Mediterranean Sea during the Holocene. Org Geochem 41:935–939

Kotthoff U, Pross J, Muller UC, Peyron O, Schmiedl G, Schulz H, Bordon A (2008) Climate dynamics in the borderlands of the Aegean Sea during formation of sapropel S1 deduced from a marine pollen record. Quat Sci Rev 27:832–845

Kouli K, Gogou A, Bouloubassi I, Triantaphyllou MV, Ioakim C, Katsouras G, Roussakis G, Lykousis V (2012) Late postglacial paleoenvironmental change in the northeastern Mediterranean region: combined palynological and molecular biomarker evidence. Quat Int 261:118–127

Kuhnt T, Schmiedl G, Ehrmann W, Hamann Y, Hemleben C (2007) Deep-sea ecosystem variability of the Aegean Sea during the past 22 kyr as revealed by benthic foraminifera. Mar Micropaleontol 64: 141–162

Kuhnt T, Schmiedl G, Ehrmann W, Hamann Y, Andersen N (2008) Stable isotopic composition of Holocene benthic foraminifers from the Eastern Mediterranean Sea: past changes in productivity and deep water oxygenation. Palaeogeogr Palaeoclimatol Palaeoecol 268: 106–115

Lagaria A, Psarra S, Gogou A, Tuğrul S, Christaki U (2013) Particulate and dissolved primary production along a pronounced hydrographic and trophic gradient (Turkish Straits System-NE Aegean Sea). J Mar Syst 119–120:1–10

Lascaratos A (1992) Hydrology of the Aegean sea. In: Charnock H (ed) Winds and currents of the Mediterranean Basin. NATO Advanced Science Institute. Atmospheric and Oceanic Circulation in the Mediterranean Basin, vol 40. Harvard University, pp 313–334

Loeblich AR, Tappan H (1987) Foraminiferal genera and their classification. Van Nostrand Reinhold, New York

Loeblich AR, Tappan H (1994) Foraminifera of the Sahul Shelf and Timor Sea. Cushman Foundation for Foraminiferal Research, Washington, spec publ 31

Lykousis V, Chronis G, Tselepides A, Price NB, Theocharis A, Siokou-Fragou I, van Wambeke F, Danovaro R, Stavrakakis S, Duineveld G, Georgopoulos D, Ignatiades L, Souvermezoglou A, Voutsinou-Taliadouri F (2002) Major outputs of the recent multidisciplinary biogeochemical researches undertaken in the Aegean Sea. J Mar Syst 33–34:313–334

Magurran AE (1988) Ecological diversity and its measurement. Princeton University Press, Princeton, NJ

Major CO, Goldstein SL, Ryan WBF, Lericolais G, Piotrowski AM, Hajdas I (2006) The co-evolution of Black Sea level and composition through the last deglaciation and its paleoclimatic significance. Quat Sci Rev 25:2031–2047

Marino G, Rohling EJ, Sangiorgi F, Hayes A, Casford JL, Lotter AF, Kucera M, Brinkhuis H (2009) Early and middle Holocene in the Aegean Sea: interplay between high and low latitude climate variability. Quat Sci Rev 28:3246–3262

Marlowe IT, Brassell SC, Eglinton G, Green JC (1984) Long chain unsaturated ketones and esters in living algae and marine sediments. Org Geochem 6:135–141

Meador TB, Gogou A, Spyres G, Herndl GJ, Krasakopoulou E, Psarra S, Yokokawa T, De Corte D, Zervakis V, Repeta DJ (2010) Biogeochemical relationships between ultrafiltered dissolved organic matter and picoplankton activity in the Eastern Mediterranean Sea. Deep-Sea Res II 57:1460–1477

Menzel D, van Bergen PF, Schouten S, Sinninghe Damsté JS (2003) Reconstruction of changes in export productivity during Pliocene sapropel deposition: a biomarker approach. Palaeogeogr Palaeoclimatol Palaeoecol 190:273–287

Mercone D, Thomson J, Croudace IW, Siani G, Paterne M, Troelstra S (2000) Duration of S1, the most recent sapropel in the eastern Mediterranean Sea, as indicated by AMS radiocarbon and geochemical evidence. Paleoceanography 15:336–347

Mercone D, Thomson J, Abu-Zied RH, Croudace IW, Rohling EJ (2001) High resolution geochemical and micropaleontological profiling of the most recent eastern Mediterranean sapropel. Mar Geol 177:25–44

Mertens KN, Bradley LR, Takano Y, Mudie PJ, Marret F, Aksu AE, Hiscott RN, Verleye TJ, Mousing EA, Smyrnova LL, Bagheri S, Mansor M, Pospelova V, Matsuoka K (2012) Quantitative estimation of Holocene surface salinity variation in the Black Sea using dinoflagellate cyst process length. Quat Sci Rev 39:45–59

Meyers PA, Arnaboldi M (2008) Paleoceanographic implications of nitrogen and organic carbon isotopic excursions in mid-Pleistocene sapropels from the Tyrrhenian and Levantine Basins, Mediterranean Sea. Palaeogeogr Palaeoclimatol Palaeoecol 266: 112–118

Mojtahid M, Jorissen FJ, Garcia J, Schiebel R, Michel E, Eynaud F, Gillet H, Cremer M, Diz Ferreiro P, Siccha M, Howa H (2013) High resolution Holocene record in the southeastern Bay of Biscay: global versus regional climate signals. Palaeogeogr Palaeoclimatol Palaeoecol 377:28–44

Müller PJ, Kirst G, Ruhland G, von Storch I, Rosell-Melé A (1998) Calibration of the alkenone paleotemperature index $U_{37}^{K'}$ based on core-tops from the eastern South Atlantic and the global ocean (60°N–60°S). Geochim Cosmochim Acta 62:1757–1772

Myers PG, Rohling EJ (2000) Modeling a 200 yr interruption of the Holocene Sapropel S1. Quat Res 53:98–104

Ohkouchi N, Kawamura K, Kawahata H, Taira A (1997) Latitudinal distributions of terrestrial biomarkers in the sediments from the Central Pacific. Geochim Cosmochim Acta 61:1911–1918

Pavlopoulos K, Kapsimalis V, Theodorakopoulou K, Panagiotopoulos IP (2012) Vertical displacement trends in the Aegean coastal zone (NE Mediterranean) during the Holocene assessed by geo-archaeological data. The Holocene 22:717–728

Pavlopoulos K, Fouache E, Sidiropoulou M, Triantaphyllou M, Vouvalidis K, Syrides G, Gonnet A, Greco E (2013) Palaeoenvironmental evolution and sea-level changes in the coastal area of NE Lemnos Island (Greece) during the Holocene. Quat Int 308–309:80–88

Pujol C, Vergnaud Grazzini C (1995) Distribution of live planktic foraminifers as related to regional hydrography and productive systems of the Mediterranean Sea. Mar Micropaleontol 25:187–217

Reimer PJ, Bard E, Bayliss A, Beck JW, Blackwell PG, Bronk Ramsey C, Buck CE, Cheng H, Edwards RL, Friedrich M, Grootes PM, Guilderson TP, Haflidason H, Hajdas I, Hatté C, Heaton TJ, Hogg AG, Hughen KA, Kaiser KF, Kromer B, Manning SW, Niu M, Reimer RW, Richards DA, Scott EM, Southon JR, Turney CSM, van der Plicht J (2013) IntCal13 and MARINE13 radiocarbon age calibration curves 0-50000 years cal BP. Radiocarbon 55:1869–1887

Repeta DJ (1989) Carotenoid diagenesis in recent marine sediments. II. Degradation of fucoxanthin to loliolide. Geochim Cosmochim Acta 53:699–707

Retailleau S, Eynaud F, Mary Y, Abdallah V, Schiebel R, Howa H (2012) Canyon heads and river plumes: how might they influence neritic planktonic foraminifera communities in the Bay of Biscay? J Foram Res 42:257–269

Rigual-Hernández AS, Sierro FJ, Bárcena MA, Flores JA, Heussner S (2012) Seasonal and interannual changes of planktic foraminiferal fluxes in the Gulf of Lions (NW Mediterranean) and their implications for paleoceanographic studies: two 12-year sediment trap records. Deep-Sea Res I 66:26–40

Rohling EJ, Pälike H (2005) Centennial-scale climate cooling with a sudden event around 8,200 years ago. Nature 434:975–979

Rohling EJ, Jorissen FJ, Vergnaud-Grazzini C, Zachariasse WJ (1993) Northern Levantine and Adriatic Quaternary planktic foraminifera; reconstruction of paleoenvironmental gradients. Mar Micropaleontol 21:191–218

Rohling EJ, Jorissen FJ, De Stigter HC (1997) 200 year interruption of Holocene sapropel formation in the Adriatic Sea. J Micropalaeontol 16:97–108

Rohling EJ, Cane TR, Cooke S, Sprovieri M, Bouloubassi I, Emeis KC, Schiebel R, Kroon D, Jorissen FJ, Lorre A, Kemp AES (2002a) African monsoon variability during the previous interglacial maximum. Earth Planet Sci Lett 202:61–75

Rohling EJ, Mayewski PA, Abu-Zied RH, Casford JSL, Hayes A (2002b) Holocene atmosphere–ocean interactions: records from Greenland and the Aegean Sea. Clim Dyn 18:587–593

Rohling EJ, Marino G, Grant KM (2015) Mediterranean climate and oceanography, and the periodic development of anoxic events (sapropels). Earth Sci Rev 143:62–97

Rosenthal Y, Morley A, Barras C, Katz ME, Jorissen F, Reichart GJ, Linsley BK (2011) Temperature calibration of Mg/Ca ratios in the intermediate water benthic foraminifer *Hyalinea balthica*. Geochem Geophys Geosyst 12, Q04003. doi:10.1029/2010GC003333

Rossignol-Strick M, Nesteroff W, Olive P, Vergnaud-Grazzini C (1982) After the deluge: Mediterranean stagnation and sapropel formation. Nature 295:105–110

Roussakis G, Karageorgis AP, Conispoliatis N, Lykousis V (2004) Last glacial–Holocene sediment sequences in N. Aegean basins: structure, accumulation rates and clay mineral distribution. Geo-Mar Lett 24:97–111

Ryan WBF, Major CO, Lericolais G, Goldstein SL (2003) Catastrophic flooding of the Black Sea. Annu Rev Earth Planet Sci 31:525–554

Schiebel R, Waniek J, Bork M, Hemleben C (2001) Planktic foraminiferal production stimulated by chlorophyll redistribution and entrainment of nutrients. Deep-Sea Res I 48:721–740

Schiebel R, Zeltner A, Treppke UF, Waniek JJ, Bollmann J, Rixen T, Hemleben C (2004) Distribution of diatoms, coccolithophores and planktic foraminifers along a trophic gradient during SW monsoon in the Arabian Sea. Mar Micropaleontol 51:345–371

Schmiedl G, de Bovée F, Buscail R, Charrière B, Hemleben C, Medernach L, Picon P (2000) Trophic control of benthic foraminiferal abundance and microhabitat in the bathyal Gulf of Lions, western Mediterranean Sea. Mar Micropaleontol 40:167–188

Schmiedl G, Kuhnt T, Ehrmann W, Emeis KC, Hamann Y, Kotthoff U, Dulski P, Pross J (2010) Climatic forcing of eastern Mediterranean deep-water formation and benthic ecosystems during the past 22, 000 years. Quat Sci Rev 29:3006–3020

Sen Gupta BK, Machain-Castillo ML (1993) Benthic foraminifera on oxygen-poor habitats. Mar Micropaleontol 20:183–201

Soulet G, Ménota G, Lericolais G, Bard E (2011) A revised calendar age for the last reconnection of the Black Sea to the global ocean. Quat Sci Rev 30:1019–1026

Sperling M, Schmiedl G, Hemleben C, Emeis KC, Erlenkeuser H, Grootes PM (2003) Black Sea impact on the formation of eastern Mediterranean sapropel S1? Evidence from the Marmara Sea. Palaeogeogr Palaeoclimatol Palaeoecol 190:9–21

Stuiver M, Reimer PJ (1993) Extended C-14 data-base and revised Calib 3.0 C-14 age calibration program. Radiocarbon 35:215–230

Tachikawa K, Vidal L, Cornuault M, Garcia M, Pothin A, Sonzogni C, Bard E, Menot G, Revel M (2015) Eastern Mediterranean Sea circulation inferred from the conditions of S1 sapropel deposition. Clim Past 11:855–867

Tao S, Xing L, Luo X, Wei H, Liu Y, Zhao M (2012) Alkenone distribution in surface sediments of the southern Yellow Sea and implications for the $U_{37}^{K'}$ thermometer. Geo-Mar Lett 32:61–71

Theocharis A, Georgopoulos D (1993) Dense water formation over the Samothraki and Limnos Plateaux in the North Aegean Sea (Eastern Mediterranean Sea). Cont Shelf Res 13:919–939

Theocharis A, Krokos G, Velaoras D, Korres G (2014) An internal mechanism driving the alternation of the Eastern Mediterranean Dense/Deep Water Sources. In: Borzelli GLE, Gačić M, Lionello P, Malanotte-Rizzoli P (eds) The Mediterranean Sea: temporal variability and spatial patterns. Geophys Monogr 202:113–137

Triantaphyllou MV (2014) Coccolithophore assemblages during the Holocene Climatic Optimum in the NE Mediterranean (Aegean and northern Levantine Seas, Greece): paleoceanographic and paleoclimatic implications. Quat Int 345:56–67

Triantaphyllou MV, Ziveri P, Gogou A, Marino G, Lykousis V, Bouloubassi I, Emeis KC, Kouli K, Dimiza M, Rosell-Mele A, Papanikolaou M, Katsouras G, Nunez N (2009a) Late Glacial-Holocene climate variability at the south-eastern margin of the Aegean Sea. Mar Geol 266:182–197

Triantaphyllou MV, Antonarakou A, Kouli K, Dimiza M, Kontakiotis G, Papanikolaou M, Ziveri P, Mortyn G, Lianou V, Lykousis V, Dermitzakis MD (2009b) Late Glacial–Holocene ecostratigraphy of the south-eastern Aegean Sea, based on plankton and pollen assemblages. Geo-Mar Lett 29:249–267

Triantaphyllou MV, Gogou A, Bouloubassi I, Dimiza M, Kouli K, Roussakis G, Kotthoff U, Emeis KC, Papanikolaou M, Athanasiou M, Parinos K, Ioakim C, Lykousis V (2014) Evidence for a warm and humid Mid-Holocene episode in the Aegean and northern Levantine Seas (Greece, NE Mediterranean). Reg Environ Change 14:1697–1712

Velaoras D, Lascaratos A (2005) Deep water mass characteristics and interannual variability in the North and Central Aegean Sea. J Mar Syst 53:59–85

Velaoras D, Kassis D, Perivoliotis L, Pagonis P, Hondronasios A, Nittis K (2013) Temperature and salinity variability in the Greek Seas based on POSEIDON stations time series: preliminary results. Med Mar Sci 14:5–18

Velaoras D, Krokos G, Nittis K, Theocharis A (2014) Dense intermediate water outflow from the Cretan Sea: a salinity driven, recurrent phenomenon, connected to thermohaline circulation changes. J Geophys Res Oceans 119(8):4797–4820

Vidal L, Ménot G, Joly C, Bruneton H, Rostek F, Çağatay MN, Major C, Bard E (2010) Hydrology in the Sea of Marmara during the last 23 ka: implications for timing of Black Sea connections and sapropel deposition. Paleoceanography 25, PA1205. doi:10.1029/2009PA001735

Volkman JK (1986) A review of sterol markers for marine and terrigenous organic matter. Org Geochem 9:83–99

Zachariasse WJ, Jorissen FJ, Perissoratis C, Rohling EJ, Tsapralis V (1997) Late Quaternary foraminiferal changes and the nature of sapropel S1 in Skopelos Basin. Proc 5th Hell Symp Oceanogr Fish 1:391–394

Zervakis V, Georgopoulos D, Drakopoulos PG (2000) The role of the North Aegean in triggering the recent Eastern Mediterranean climatic changes. J Geophys Res 105:26103–26116

Zervakis V, Georgopoulos D, Karageorgis AP, Theocharis A (2004) On the response of the Aegean Sea to climatic variability: a review. Int J Climatol 24:1845–1858

Zodiatis G (1994) Advection of the Black Sea Water in the North Aegean Sea. Glob Atmosph Ocean Syst 2:41–60